Design Science

Design and manufacture of hybrid metal composite structures using functional tooling made by additive manufacturing

Daniel-Alexander Türk[1], Fabian Rüegg[2], Manuel Biedermann[2] and Mirko Meboldt[2]

1 *California Institute of Technology, Pasadena, CA, USA*
2 *ETH Zürich, Zürich, Switzerland*

Abstract

This paper presents a novel manufacturing technique for complex-shaped, hybrid metal composite structures leveraging the design freedom of additive manufacturing (AM). The key novelty of this research is an approach for an autoclave-suitable and removable tooling, which consists of a 3D-printed functional shell and a structural filler material. In this process, a layup shell is produced with AM and filled with a temperature-resistant curing support to form a removable inner tooling. The functional shell has integrated design features for the positioning and the fixation of metallic interface elements and is removed after curing through integrated breaking lines. The feasibility of this manufacturing technique is demonstrated by fabricating a novel lightweight structure for the hydraulic quadruped (HyQ) robot. Selective laser sintering (SLS) was used to produce the functional shell tooling. Titanium interface elements made via selective laser melting (SLM) were assembled to the shell and co-cured to carbon fiber using an autoclave prepreg process. The resulting multi-material structure was tested in ultimate strength and successfully operated on the HyQ robot. Weight savings of 55% compared to a reference design and the mechanical viability of the multi-material structure indicate that the proposed manufacturing technique is appropriate for individualized hybrid composite structures with complex geometries.

Key words: lightweight design, additive manufacturing, multi-material structures, carbon-fiber composite

Received 12 December 2018
Revised 25 July 2019
Accepted 12 August 2019

Corresponding author
D. Türk
daniel.tuerk@outlook.com

Published by Cambridge University Press

Des. Sci., vol. 5, e16
journals.cambridge.org/dsj
DOI: 10.1017/dsj.2019.16

1. Introduction

Metallic tooling is widely used as a shape-giving support in most manufacturing techniques for high-performance composite structures, including autoclave curing (Fernlund *et al.* 2002), filament winding (Lossie & Van Brussel 1994), or bladder molding (Bernet *et al.* 2001). Despite achieving good surface quality, low micro-structural defects, and excellent structural performance, composite parts fabricated using these processes are generally limited in geometrical complexity as their manufacturability is bound to the capability of the tooling. As a consequence, composite parts often do not achieve the full lightweight potential. Traditional tooling is typically machined and assembled and, therefore, characterized by long lead times, representing a major up-front non-recurring cost, especially

for low volume series. Moreover, tooling may require continual maintenance and modifications dependent on the design and the variety of produced parts (Campbell 2003).

The trend toward integrated, high-performance composites with complex shapes demands for manufacturing techniques with increased design freedom and flexibility. Recently, additive manufacturing (AM) has been increasingly used for the production of metallic and polymeric tools and molds for various manufacturing process chains (e.g. injection molding). AM encompasses a set of production technologies allowing complex geometries to be created from digital models. The process works, in general, by solidifying or depositing material layer by layer only where required to build a three-dimensional (3D) part (ASTM Std. F2792-12a 2012). Previous studies demonstrated the added value of unprecedented AM design solutions which improve the performance of the part in terms of weight savings (Orme *et al.* 2017), heat transfer (Dede, Joshi & Zhou 2015), or fluid flow (Schmelzle *et al.* 2015), to name a few. On the processing side, AM has a clear potential in the cost-effective production of functional and complex-shaped tools. Among others, binder jetting has been identified as a promising technique for rapid sand-casting applications. Critical parameters such as gas permeability, strength, and heat absorption are defined during the design process and directly manufactured, resulting in a functional, light, and low-cost mold (Upadhyay, Sivarupan & El Mansori 2017). AM functional tools can also complement established manufacturing process chains to achieve parts with very specific requirements. For example, the replication quality of features on the micro-scale is limited using traditional injection molding processes. Zhang et al. have proposed a soft tool with micro-features made by vat photo-polymerization, a high-resolution 3D-printing technique. The soft tool is inserted during the injection molding process to replicate the micro-features onto the molded part (Zhang *et al.* 2017).

AM has also been adopted in the production of tools for the prototyping and fabrication of composite parts (Black 2015; Türk *et al.* 2017). A major consideration in the layup processing of thermoset composites is the curing step, where elevated temperatures and pressures are applied over time. Therefore, major research activities focus on the development of thermally stable thermoplastic materials and their characterization for the processing with composites (Li *et al.* 2015; Lušić, Schneider & Hornfeck 2016; Duty *et al.* 2017). Researchers at Oak Ridge National Laboratory have proposed to reinforce thermoplastic beads with carbon-fiber loadings to improve the thermo-mechanical properties for 3D printing of in-autoclave tooling (Hassen *et al.* 2016; Stratasys Ltd. 2017*a*). Stratasys Ltd. has presented an updated design guideline for composite tooling using fused deposition modeling and is commercializing a thermoplastic blend (St-130) material for soluble tooling which is chemically dissolved in an alkaline solution (Stratasys Ltd. 2017*b*). Ma *et al.* (2007) reported that filling thermoset epoxy composites with alumina powder increases the thermo-mechanical properties and may be suitable for rapid tooling applications.

In previous research, we have proposed two manufacturing techniques for the autoclave processing of hybrid lightweight structures. Here, we define hybrid structures as multi-material structures on the macroscopic level which are combined from different materials using a specific process. In the first approach, ST-130 material was used to produce soluble in-autoclave tooling for a novel lower

https://doi.org/10.1017/dsj.2019.16 Published online by Cambridge University Press

limb prosthesis (Türk *et al.* 2018). Although this approach yielded a mechanically viable and lightweight product, the approach presented shortcomings in terms of ST-130 material cost, availability, thermo-mechanical stability, and excessive material usage. In the second approach, a water-soluble sand core was produced with binder jetting, over-laminated with carbon-fiber reinforced polymers (CFRP), and cured in the autoclave. The approach was applied to the lower leg structure of the hydraulic quadruped (HyQ) robot developed at the Italian Institute of Technology (Semini *et al.* 2011). The resulting structure consisted of load introduction elements made with selective laser melting (SLM) which were co-cured to pre-impregnated (prepreg) CFRP. Weight savings greater than 50% highlight the potential of this approach for hollow and complex-shaped hybrid lightweight structures (Türk, Triebe & Meboldt 2016). However, the sand core approach presented limitations with regard to material brittleness, insufficient sealing quality, and most importantly the coarse printing resolution which limits the possibility for the integration of design features. As a result, the approach is not suitable for highly intricate structures with high geometrical complexity.

This paper presents a novel manufacturing technique for complex-shaped, hybrid composite structures eliminating the shortcomings of previous approaches. It allows the manufacturing of hollow composite and hybrid composite structures using an autoclave prepreg curing process, while keeping the tooling effort (lead time and costs) low and allowing for design variants through AM design adoptions. In this technique, a polymer shape-giving shell is produced with AM and filled with a temperature-resistant filler material prior to the lamination of the reinforcements. In addition, metal AM is used to produce structural lightweight components which are integrated during the layup of the reinforcements. After curing, the filler material is removed and the polymeric shell is peeled out, resulting in a highly integrated and complex-shaped composite part. The approach is applied to the lower leg structure of the HyQ robot, which is fabricated, mechanically verified, and successfully operated on the robot.

This paper is organized as follows. Section 2 outlines the generalized manufacturing technique. Section 3 describes the design and manufacturing of the robot leg structure using the novel manufacturing technique. Section 4 presents the results. Section 5 discusses the approach in a wider context and Section 6 concludes the paper.

2. Manufacturing technique

This section presents a manufacturing technique for complex-shaped, hybrid composites. Any composite tooling requires to provide the shape of part to be built, the structural support to withstand curing conditions, and the necessary functionality to position and fix load introduction elements. In most traditional and recent AM tooling, these three functions are combined in one singular part yielding high cost, long lead times, and/or high material usage (Morena 2011). The key feature of the proposed technique originates from function-based methodologies developed by Kirschman & Fadel (1998) which, in this context, is expressed as a separation of the three aforementioned functions as follows: An additive manufactured shell provides the layup surface for the part shape and integrated design features supporting the manufacturing or the operation of the part. A filler material acts as a temporary structural curing support during pressure and temperature loading. Both are removed after curing, resulting in a

https://doi.org/10.1017/dsj.2019.16 Published online by Cambridge University Press

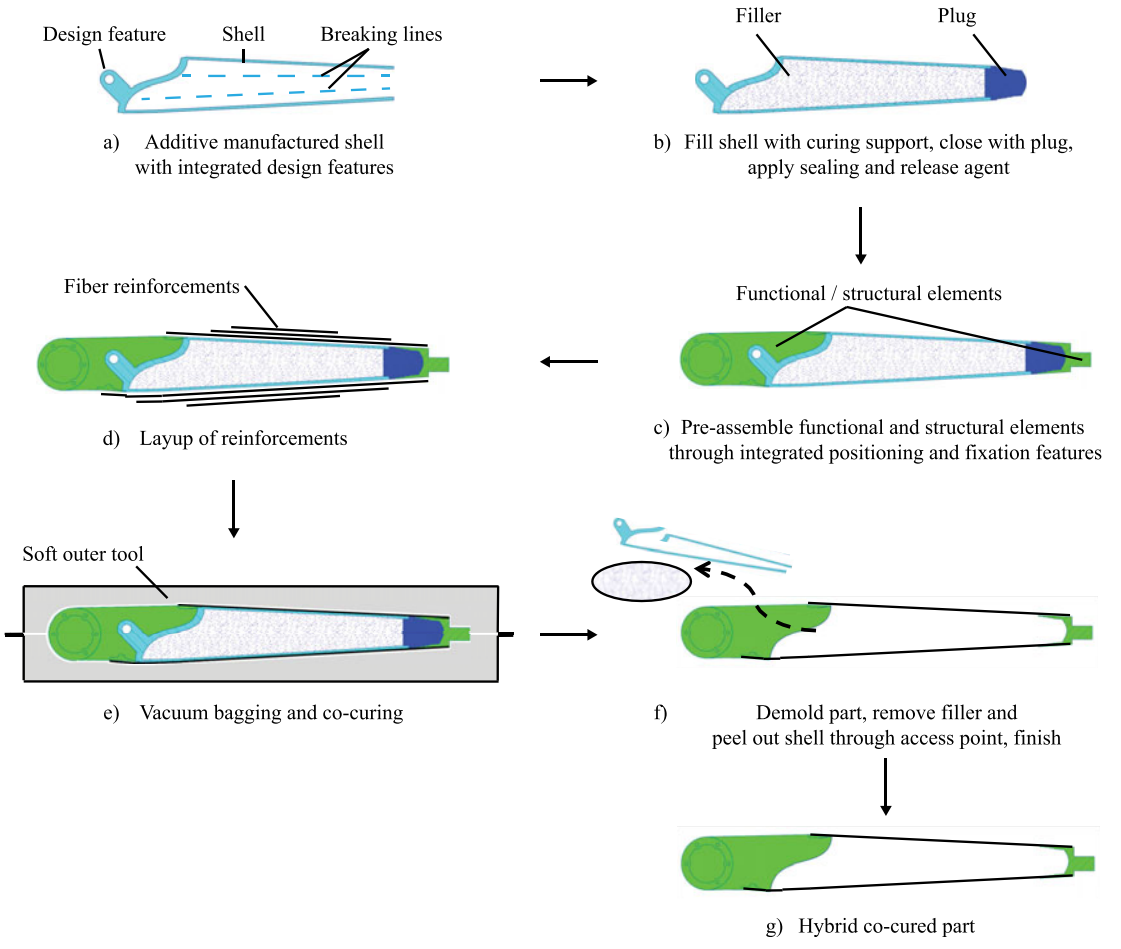

Figure 1. Manufacturing technique for complex-shaped hybrid composites using a functional 3D-printed shell (a) which is filled with a structural curing support (b) and pre-assembled with functional elements (c). Reinforcement fibers are laid on the assembly (d) which bagged and cured (e). After curing, the part is demolded, the filler is removed, and the shell is peeled out (f), resulting in a hybrid composite part (g).

complex part. Hence, a function-driven tooling approach is chosen on multiple levels. The first level is the separation of functions as mentioned previously, which is a key novelty in the context of tooling. Second, leveraging the design freedom of AM allows the integration of additional functional features within the tooling shell. The manufacturing technique is depicted in Figure 1 and the major steps are described in the following subsections.

2.1. Shell tooling

A thin 3D-printed polymeric shell provides the complex layup surface and thus the inner contour of the hollow composite part to be built (Figure 1a). In addition, defined design features may be integrated into the shell to add specific functions to it. Here, design features are defined as data which is related to the design object and may refer to shape, material, tolerance, or other functional aspects of

https://doi.org/10.1017/dsj.2019.16 Published online by Cambridge University Press

the part (Ovtcharova, Pahl & Rix 1992). They may support the manufacturing or the operation of the part, and examples include positioning and fixation interfaces for the assembly of additional elements. The shell thickness should be selected such that the shell can easily be removed in the subsequent process steps while providing sufficient stability during the filling and the curing step. Bulging should be avoided during filling and curing pressure should not lead to shell collapse. After curing, the shell is removed along integrated breaking lines which correspond to local thickness reductions in the shell.

2.2. Fill shell and enclosure

The shell is filled with a filler material and closed with one or multiple 3D-printed plugs (Figure 1b). The main function of the filler material is to provide a temporary structural support during curing of the part in a fiber-reinforced polymer (FRP) manufacturing process, where elevated temperature and pressure are applied over time. The following requirements for the filler material are proposed. First, the filler may be a granular material with good flowability when poured into complex volumes with undercuts. The grain size and the grain size distribution may be considered to successfully fill hollow spaces with detailed geometric features. In addition, the filler material should withstand elevated curing loadings. Therefore, it ideally is temperature-resistant, exhibits a coefficient of thermal expansion close to the one of the part, and has adequate stiffness in compression. Moreover, the material should be widely available and cost-efficient. The plug is a critical interface element to enclose the filler in the hollow body shell. It may be produced with the same manufacturing technique as the shell to ensure compatibility. The interface of the plug to the shell is critical and should be designed as press fit to prevent resin inflow during curing. A temperature-resistant sealant is applied to the outer volume comprising the shell and the plug to prevent resin inflow during curing. Additional surface operations (e.g. sanding) may be conducted to improve the surface quality prior to sealant application. The sealant also acts as a basis for the release agent which allows to remove the tool (surface) from the cured part. In this research, we definte the inner tooling as the assembly of the elements that fulfill the tooling function, which in this research consists of the assembled, enclosed and sealed shell with the filler material inside of it.

2.3. Pre-assembly

One advantage of the technique is the possibility to pre-assemble complex functional and structural elements with the tooling prior to the layup of the FRP and thus prepare the hybridization of the structure (Figure 1c). Pre-assembly occurs through design features which are integrated into the shell or the plug and into the counter-parts. Here, we distinguish structural and functional elements. Structural elements are relevant to the load-bearing capability of the hybrid part and include inserts, load introduction interfaces, and fixation elements. Functional elements provide specific additional functionalities for either the operation of the part or its manufacturing and are not relevant to its primary load-carrying capability. Functional elements relevant to the part operation may consist of housing, fixations, pockets, cable ducts, and venting hoses, to name a few. Manufacturing elements support the processing which may be particularly challenging for complex parts. Among others, they include layup and handling

https://doi.org/10.1017/dsj.2019.16 Published online by Cambridge University Press

aids, positioning and fixation elements, structural curing aids and post-processing aids (Türk *et al.* 2017).

2.4. Layup

In the layup step, the reinforcements are cut in the desired orientation to (near) net shape and sequentially draped on the pre-assembled tool according to the ply book (Figure 1d). Pre-impregnated (prepregs) FRP may be used for autoclave or out-of-autoclave processing as well as semi-finished fiber products such as those employed in resin transfer molding, filament winding, and wet layup technique. The layup surfaces should meet draping requirements in order to build a complex shape without defects with a fiber alignment that is suitable for structural loads. Also, high fiber volume content should be guaranteed over the whole part.

2.5. Bagging and curing

A vacuum bagging is conducted prior to curing and may include a bleeder, a breather, and a release film, dependent on the specific application (Figure 1e). A soft outer tool may be used to enhance the pressure distribution on the layup during curing. The outer tool may be realized from master models which may be produced with AM. The composite is cured according to the selected composite processing route. In this research, the emphasis is placed on the autoclave prepreg curing technology as it is a robust state-of-the-art technique for the production of high-performance CFRP parts. In this process, prepregs are cured in the autoclave where elevated pressure and temperature is applied to consolidate the layup. This process allows to achieve CFRP parts with high fiber volume content and low porosity (Gutowski 1997). Moreover, the process allows to produce low to medium volume parts with varying geometries. It should be noted that the proposed manufacturing technique is not limited to autoclave curing and may be extended to other composites manufacturing processes. The composite may be co-cured or co-bonded to solid interface elements to form an intrinsic hybrid structure as proposed by Kießling *et al.* (2018) and Nieschlag *et al.* (2018). Co-curing composites are considered to be efficient as both the curing and the joining process for the composite are achieved simultaneously (Shin, Lim & Lee 2003). Co-curing does not require an adhesive as the excess resin is extracted from the composite material during consolidation. Alternatively, co-bonding may be used to increase the load-carrying capability of the joint by inserting an adhesive layer between the metallic and the composite adherend during layup. Consider the difference in electrode potential of both adherends and take measures to avoid contact corrosion if required.

2.6. Remove tool and post-process

After completion of the curing cycle, the soft outer tool is removed (Figure 1f). The shell is mechanically opened (e.g. drilling) at one or multiple access points to remove the filler material. The shell is peeled out along integrated breaking lines which allow for sequential removal of the shell. The plug is removed mechanically. Key to successful core removal is the consideration of the access points during the design phase. Finally, finishing operations may be applied to finalize the part. The resulting structure is hybrid, co-cured, complex-shaped, and highly integrated

https://doi.org/10.1017/dsj.2019.16 Published online by Cambridge University Press

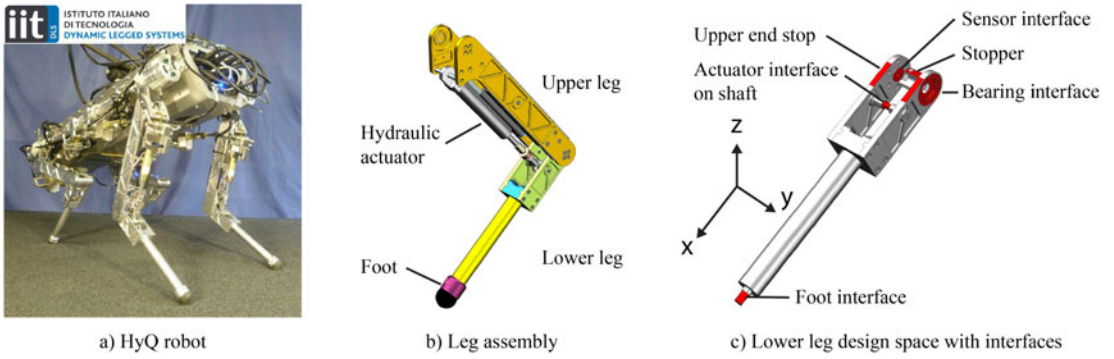

a) HyQ robot b) Leg assembly c) Lower leg design space with interfaces

Figure 2. Hydraulic quadruped (HyQ) robot (a), leg assembly (b), and lower leg design space (c); adapted from Semini *et al.* (2011) and IIT (2018).

(Figure 1g). Ideally, the structure is lightweight and exhibits the complex geometry required to optimally perform in the designated operation.

3. Experimental

3.1. Reference structure

The HyQ robot was developed at the Italian Institute of Technology (Figure 2a). HyQ is able to perform highly dynamic motions such as running, jumping, and trotting. Moreover, HyQ can navigate over rough terrain. HyQ weighs approximately 80 kg and measures 1 m in length (Semini *et al.* 2011). The four legs are hydraulically actuated and are composed of upper and lower leg assemblies (Figure 2b). In this research, the lower leg is redesigned using the manufacturing technique presented in Section 2, focusing on weight reduction while guaranteeing structural integrity. Reducing the weight and the mass moment of inertia in actuated masses may increase the robot's performance and reduce the power requirements. Figure 2c shows the design space of the lower leg which consists of six main structural elements, one shaft, two bushings, two disc springs on the shaft, and 18 bolts. Without the foot, the lower leg weighs 660 g. The six structural elements are made from aircraft grade aluminum and the shaft is made from high-performance steel. The reference design has been iterated for weight reduction and robustness.

3.2. Loading conditions

Four main maneuvers are conducted with the HyQ. In the (i) walking trot maneuver, the robot moves forward with a velocity of up to 2 m s^{-1}. In the (ii) flying trot, the robot moves diagonal leg pairs together with an average velocity of 1.5 m s^{-1}. The robot lifts off completely between the steps and lands on two diagonal legs, introducing critical peak loads into the structure. Other maneuvers are (iii) the squat jump which consists of a vertical jump of approximately 0.15 m height and (iv) the shin collision in which the robot overcomes random obstacles leading to collisions (Semini *et al.* 2011; IIT 2018). The ground reaction forces are extracted from experimental data sets and transformed into a local coordinate system to estimate the loads for the lower leg structure. Based on the experimentally measured loads, a conservative load case envelope of eight

https://doi.org/10.1017/dsj.2019.16 Published online by Cambridge University Press

Table 1. Load envelope comprising eight load cases

Load case	$F_{x,\mathrm{loc}}$ (N)	$F_{y,\mathrm{loc}}$ (N)	$F_{z,\mathrm{loc}}$ (N)
LC-1 (compression, bending 5°)	−1100	92	1046
LC-2 (compression, bending 25°)	−1100	444	952
LC-3 (compression, bending 45°)	−1100	743	743
LC-4 (tension, bending 5°)	290	92	1046
LC-5 (tension, bending 25°)	290	444	952
LC-6 (tension, bending 45°)	290	743	743
LC-7 (compression, bending −65°)	−1100	−550	256
LC-8 (tension, bending −65°)	290	−550	256

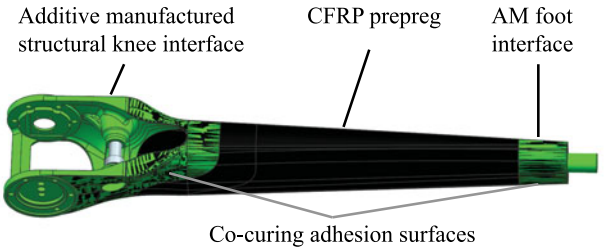

Figure 3. Design concept for the hollow multi-material part using additive manufacturing for structural and functional interfaces and a load-bearing shell made of composite materials.

individual load cases is derived (Table 1). For example, load case 1 (LC-1) consists of a superposition of the maximum compression force $F_{x,\mathrm{loc}} = -1100$ N with the maximum bending load $F_{B,\max} = 1050$ N which acts at an angle of 5° from the local z-axis. Applying the formula $F_{B,\max} = \sqrt{(F_{y_{\mathrm{loc}}})^2 + (F_{z_{\mathrm{loc}}})^2}$ to LC-1 results in $F_{B,\max}^{5°} = \sqrt{(92)^2 + (1046)^2} = 1050$ N. The other load cases were calculated accordingly.

3.3. Design concept

A multi-material design concept combining additive manufactured structural elements with high-performance CFRP prepreg is proposed. The design concept combines the strengths of both AM and the prepreg layup technologies in accordance with Ashby's guideline for hybrid material selection (Ashby & Bréchet 2003). CFRP are materials with outstanding stiffness- and strength-to-weight ratios if the fibers are oriented in the direction of the load. Therefore, they are appropriate for light, load-bearing, shell structures. AM, on the other hand, allows to realize 3D design features with a defined geometry which is promising for complex functional and structural elements such as load introductions and interfaces (Love *et al.* 2014; Türk, Klahn & Meboldt 2015). The promise of AM with CFRP is the realization of highly efficient structures by (i) realizing more efficient and more complex lightweight designs, (ii) reducing the part count through integral design, (iii) saving material through optimized load paths, and (iv) integrating additional functionalities through multi-functional design (Türk *et al.* 2015). Figure 3 shows the design concept for the lower leg structure.

https://doi.org/10.1017/dsj.2019.16 Published online by Cambridge University Press

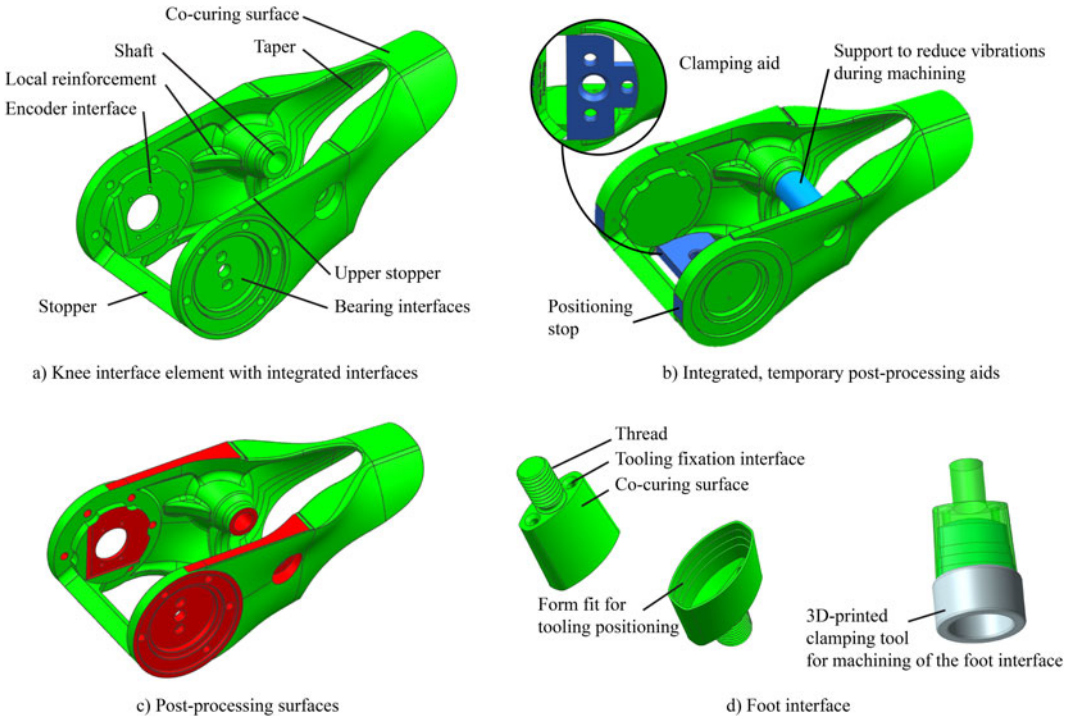

Figure 4. Structural knee- and foot-interface elements with integrated features for processing and operation.

In this concept, structural elements are produced with AM to realize an optimal load-carrying 3D shape while providing assembly interfaces and ensuring the range of motion of the system. CFRP prepregs provide an efficient lightweight structural integrity over the length of the lower leg. The CFRP is co-cured to the AM parts.

3.4. Structural AM elements

Figure 4 shows the detailed design of the structural knee-interface (a) and the foot-interface (d) elements which are designed to be manufactured with SLM. A key feature of AM is the integration of additional functionalities (Gibson, Rosen & Stucker 2010; Tang, Hascoet & Zhao 2014). The knee-interface element is a highly complex part featuring an integrated hard stopper to prevent the lower leg from additional damage in the case of software failure. Moreover, interfaces for the bearings and encoders are considered during the design. Particular attention is placed on the adhesion surface which is critical to transfer the loads from and into the CFRP. It is iteratively optimized to minimize stress peaks to allow for co-curing instead of bonding. The inner side is tapered to reduce the stiffness discontinuity in the transition area of the SLM part to the CFRP which also serves as a form fit to position the 3D-printed tooling shell.

Post-processing operations may significantly increase the total cost of the SLM part (Atzeni & Salmi 2012). Therefore, they should be considered during the design. In this research, temporary post-processing supports are integrated into the blank part (b) by including a clamping aid and a solid shaft to reduce the

https://doi.org/10.1017/dsj.2019.16 Published online by Cambridge University Press

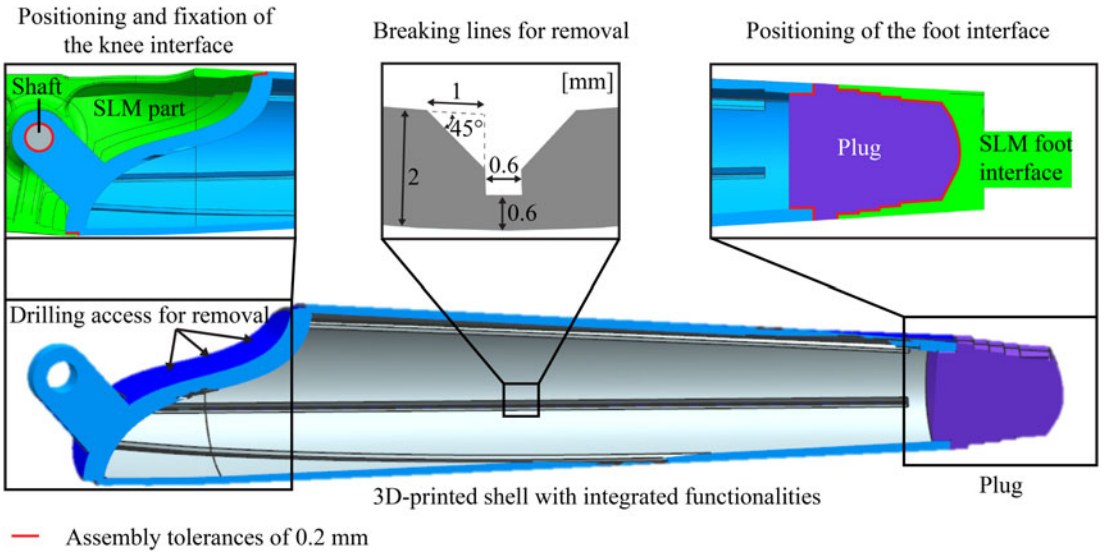

Figure 5. Additive manufactured shell with integrated design features including interfaces and breaking lines for post-cure removal of the shell.

vibrations during machining. Moreover, a position stop is integrated, supporting the positioning of the part during post-processing. This allows to machine the part from two planes only (c). First, the upper stopper surfaces are machined for flatness and parallelism. In the same step, the inner encoder interface is machined from the top. Then, the bearing surfaces and the shaft are machined from the side, allowing for an efficient post-processing procedure without having to re-clamp the part. The foot interface (d) consists of a thin SLM shell with a blank cylinder at its end. The outer surface is co-cured to the CFRP. Form fits are integrated into the inner surface to position the foot interface to the clamping aid and two screw holes allow for its fixation. The clamping aid is circular to allow for lathing of the thread including a relief groove. The fixation is removable and the clamping aid is reusable to account for small series production. During pre-assembly, the inner form fits are also used to position the foot interface to the 3D-printed tooling shell.

3.5. Tooling

The tooling concept shown in Figure 5 consists of a 3D-printed shell providing the layup surface for the CFRP, the necessary interfaces for the pre-assembly, and post-processing features. The general shell thickness amounts to 2 mm to prevent deformations during filing of the support material. Pre-assembly features include holes for the positioning of the shaft and complex form fits for the positioning of the SLM parts. Tolerances of 0.2 mm are considered at the assembly interfaces (shown in red in Figure 5) to take into account the manufacturing inaccuracies of selective laser melting and sintering. Post-processing features consist of multiple longitudinal breaking lines which allow for shell removal after curing. The shell thickness is reduced to 0.6 mm to create stress peaks during mechanical removal loading. The stress peaks result from a geometric effect which can be scaled and adapted to various shell geometries.

https://doi.org/10.1017/dsj.2019.16 Published online by Cambridge University Press

Table 2. Material properties, where [a] is as-built, [b] is the upright building direction and [c] is the averaged value from SGL Group (2018) and Concept Laser (2018)

Material	Parameter	Value	Unit
Ti6Al4V	Young's modulus[a]	110	GPa
	Poisson ratio[c]	0.33	
	Yield strength[ab]	989	MPa
	Tensile strength[ab]	1071	MPa
UD	Layer thickness	0.14	mm
	Young's modulus 0°, tension	140	GPa
	Young's modulus 90°, tension	8.4	GPa
	Shear modulus	5200	GPa
	Poisson ratio	0.32	
	Tensile strength 0°	2400	MPa
	Inter-laminar shear strength	90	MPa
Fabric	Layer thickness	0.19	mm
	Young's modulus 0°, tension	62	GPa
	Young's modulus 90°, tension	60	GPa
	Shear modulus	4670	GPa
	Poisson ratio	0.3	
	Tensile strength 0°	950	MPa
	Tensile strength 90°	900	MPa
	Inter-laminar shear strength	68	MPa
Steel	Young's modulus	220	GPa
S355J2C	Shear modulus	84	GPa
	Poisson ratio	0.31	
	Yield strength	355	MPa
	Tensile strength	470	MPa

3.6. Materials and layup

Material properties are summarized in Table 2. The composite layup consists of several layers of uni-directional (UD) SIGRAPREG C U150-0/NF-E34038% carbon-fiber prepreg with epoxy resin and twill fabric SIGRAPREG C W200-TW2/2-E323/45% manufactured by SGL Group (2018). The general layup concept consists of UD layers in areas which are mainly loaded in tension and compression, while twill layers oriented at ±45° are placed in areas with significant shear loading. Local CFRP reinforcements are patched in critical areas including the transition from the CFRP to the knee-interface part. An offset is considered in circumferential direction to provide a taper. A symmetric layup is defined at the top and bottom: The first fabric ply is oriented in 0-direction (0_f) and the second one is placed at 45°, denoted as $(45)_f$, followed by three UD plies at 0° (0_{UD}). The layup is symmetric amounting to a total of 10

https://doi.org/10.1017/dsj.2019.16 Published online by Cambridge University Press

Table 3. Design allowables, where [a] refers to conservative values for the fatigue strength and based on single-lap shear test experiments

Material	Allowable	Value	Unit
TiAl6V4	Static strength	930	MPa
	Fatigue strength	500	MPa
	Static safety factor	1.5	
	Dynamic safety factor[a]	1	
UD	Strain parallel	0.4	%
	Strain transverse	0.4	%
Fabric	Strain parallel	0.4	%
	Strain transverse	0.4	%
Adhesion	Adhesion strength[a]	8	MPa

plies: $(0_f/45_f/0_{UD}/0_{UD}/0_{UD})_s$. On the sides, the layup is defined as follows: $(0_f/0_f/45_f/0_{UD})_s$ amounting to a total of eight plies. The knee-interface parts are made from Ti6Al4V alloy processed with SLM due to excellent strength-to-weight properties of around 260 kNm kg^{-1} (Concept Laser 2018). The shaft is made from S355J2C steel.

3.7. Numerical model

A static linear-elastic simulation model was built in Abaqus to verify the structural performance of the hybrid part. The design allowables were defined to ensure the structural integrity of the leg for the entire lifetime (Table 3). The static strength of TiAl6V4 was conservatively derived from the material properties. A conservative value for the fatigue strength was chosen based on the assumption of a total of 10^6 load cycles for TiAl6V4 processed with SLM (Gong *et al.* 2012; Hosseini 2012). Safety factors for static and fatigue loading were defined to 1.5 and 1, respectively.

The structural integrity of the CFRP was assessed using a maximum strain criterion amounting to 0.4% strain for static and fatigue loading. This factor is conservative, employed in aircraft industry, and already includes poor hot-wet notched compression performance and post-impact requirements. The co-cured adhesion area may be critical to the structural integrity of the hybrid part. Therefore, the allowable was set to 8 MPa, a conservative value. The single-lap shear strength of co-cured CFRP-Ti6Al4V joints was characterized in internally conducted tests and amounted to approximately 13 MPa. Therefore, a safety factor of 1.68 was achieved.

The finite element method (FEM) model in Figure 6 includes the two titanium parts and the CFRP layup. The titanium parts were modeled using tetrahedral solid elements with quadratic shape functions (C3D10), and for the CFRP S4R, general-purpose shell elements were employed. The CFRP shell and the AM parts were tied, assuming to be non-separable without any relative displacement. This assumption serves as a first approximation for the global behavior of the structure. Reference points and kinematic coupling was used to apply the constraints. The bearing interfaces were fully constrained except for the rotation around the local

https://doi.org/10.1017/dsj.2019.16 Published online by Cambridge University Press

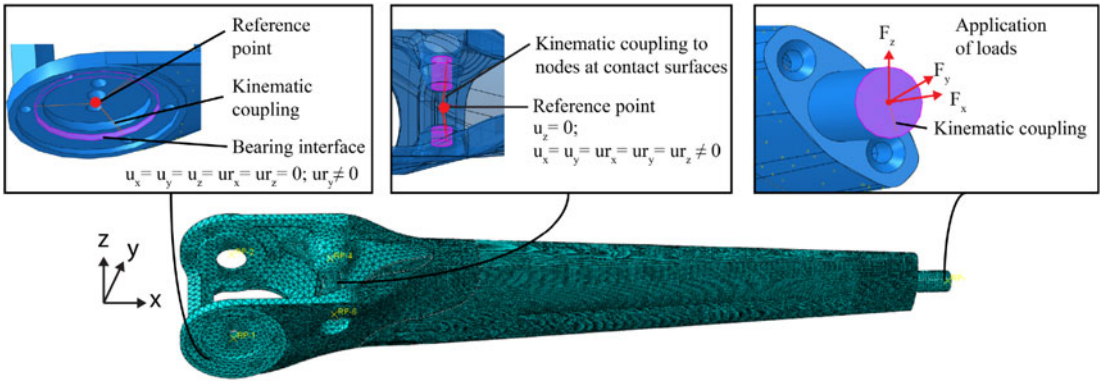

Figure 6. Numerical simulation model for the structure using Abaqus. The composite is tied to the interface elements.

y-axis. The influence of the shaft was taken into account by limiting the movement of the corresponding nodes at the contact surfaces and fixing their displacement in the local z-direction through a reference point and kinematic coupling. The loads were introduced as concentrated forces using a reference point which was coupled to the lower surface of the foot insert. The foot consists of a spherical rubber which allows to introduce forces but no moments, and, therefore, it was idealized as a point contact with forces only.

3.8. Manufacturing

The lower leg was fabricated according to the generalized manufacturing technique presented in Section 2. The tooling (comprising the shell and the plug) was produced from DuraForm HST Composite (3D Systems 2018) using selective laser sintering on a DTM Sinterstation 2500plus with a part bed temperature of 170 °C, laser power of 48 W, scan speed of 10 m s^{-1}, and a hatch distance set to 0.24 mm. SLS was selected due to its relatively high accuracy (Salmi *et al.* 2013), potential cost-efficiency for high-variety manufacturing (Fontana, Marinelli & Meboldt 2017), and its freedom of design. Also, the HST material is commercially available and exhibits acceptable thermo-mechanical properties (Türk *et al.* 2017). The filler material consisted of commercially available table salt which was filled into the shell and compacted by shaking and tapping. Salt is a granular material, exhibits a high compression modulus, has a melting temperature of up to 800 °C (Sriapai, Walsri & Fuenkajorn 2012), is inexpensive, and is widely available. The plug was produced with SLS and enclosed the inner volume of the shell. The plug and the shell were bonded using J-B Weld, a high temperature two-component epoxy system. In the next step, the tool was sealed to prevent resin inflow during curing. Note that sealing is critical to achieve satisfactory surface quality and mechanical performance at the inner surface of the CFRP, where post-processing may not be feasible and quality inspection may be difficult. The resin MGS L 235 and the corresponding hardener were manually applied using a roller and cured at room temperature to seal the tool. Next, a standard release agent (Axel XTEND 832) was applied to allow tool–part release after curing.

The SLM parts were produced from Ti6Al4V on a Concept LaserCusing machine by 3D Precision SA, Switzerland. The parts were removed from the

https://doi.org/10.1017/dsj.2019.16 Published online by Cambridge University Press

Figure 7. Machining of the 3D-printed titanium knee-interface element.

building platform. The bonding surfaces were covered during the sand-blasting operation to retain the as-built surface roughness. To relieve residual stresses, the parts were heat-treated in a chamber filled with argon gas. The parts were heated at a rate of 5 °C min^{-1}, held for 2 h at 840 °C, and cooled down at a rate of 1 °C min^{-1} to 500 °C, resulting in a total cycle time of 12 h. To account for part errors due to thermal deformation (Paul, Anand & Gerner 2014), a positive material offset of 1 mm was considered on relevant functional surfaces of the SLM parts. In the next step, the SLM parts were machined for functional surfaces and tolerances. The knee interface was screwed to a counter-part using the integrated clamping aid (Figure 7) which acted as a reference surface and allowed for automated machining. In the last machining step, the vibration support was removed. The foot interface was attached to the 3D-printed machining tool, and the thread and the groove were lathed.

The separate parts consisting of two structural SLM elements and the sealed tooling were assembled using the integrated positioning and fixation features of the 3D-printed tooling, as shown in Figure 8a. The knee interface was fixed using the shaft and the foot interface was fixed using bolts. Adhesive tape was applied to functional surfaces to avoid resin contamination. The prepreg material was cut to the desired shape and laid down on the pre-assembled tool according to the layup defined in Section 3.6 (b). The entire assembly was placed in a two-part silicone outer mold. ProtoSil RTV 245 silicone from Altropol (Altropol 2018) was cast into a 3D-printed master mold to form the outer soft tooling. The silicone mold should support the compaction of the CFRP, improve the pressure distribution, and minimize wrinkles (c). The assembly was vacuum bagged (d) and cured in the autoclave: The assembly was heated at a rate of 1 °C min^{-1} up to 100 °C, held for 300 min, and cooled down at a rate of 1 °C min^{-1}. Vacuum and 2 bar autoclave pressure were applied.

After curing, the following steps were taken to finalize the part (e). First, the shafts and the bolts were removed which were required for the fixation of the tooling. Then, a hole was drilled into the shell to access the salt. The shell was completely emptied from the salt. Finally, the shell was removed piece by piece using a plier. The shell successfully broke along the intended breaking lines.

https://doi.org/10.1017/dsj.2019.16 Published online by Cambridge University Press

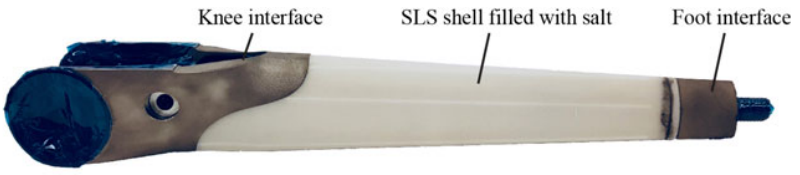

a) Pre-assembled shell with SLM parts

b) Layup of CFRP prepregs

c) Enclose assembly in outer silicone mold

d) Vacuum bagging and autoclave curing

e) Tool removal: Drilling through shell, salt removal and mechanical removal of shell

Figure 8. Manufacturing technique combining a 3D-printed shell and structural elements with carbon-fiber prepreg composite for autoclave processing.

https://doi.org/10.1017/dsj.2019.16 Published online by Cambridge University Press

Figure 9. Hybrid co-cured composite structure with integrated structural titanium interfaces (left) and during operation on the HyQ robot at the Italian Institute of Technology in Genova.

Table 4. Von Mises stresses in the knee interface and logarithmic laminate strains in the composite for different load envelopes

Load case	Von Mises stress (MPa)	Strain in composite (%)
LC-1 (compression, bending 5°)	462	0.25
LC-2 (compression, bending 25°)	458	0.29
LC-3 (compression, bending 45°)	425	0.30
LC-4 (tension, bending 5°)	485	0.26
LC-5 (tension, bending 25°)	489	0.30
LC-6 (tension, bending 45°)	439	0.31
LC-7 (compression, bending −65°)	253	0.19
LC-8 (tension, bending −65°)	227	0.17

The plug was removed from the part by applying a force through the two bore holes of the foot interface. Finally, surface finishing operations were applied. The resulting structure is an intrinsic hybrid lightweight structure, as the hybridization occurred during the curing process. The structure is complex-shaped and hollow. It was mounted on the HyQ robot (Figure 9) and successfully operated through a set of highly dynamic maneuvers.

4. Results

4.1. Simulation results

The load envelope consisting of eight load cases was numerically analyzed for structural substantiation. Table 4 shows the maximum Von Mises stresses in the knee-interface element and the maximum in-plane strain in the composite laminate. The simulation revealed that combined tension and bending loading at 25° (load case 5) yields stresses amounting up to 489 MPa located in the bearing seats of the knee interface (Figure 10a).

https://doi.org/10.1017/dsj.2019.16 Published online by Cambridge University Press

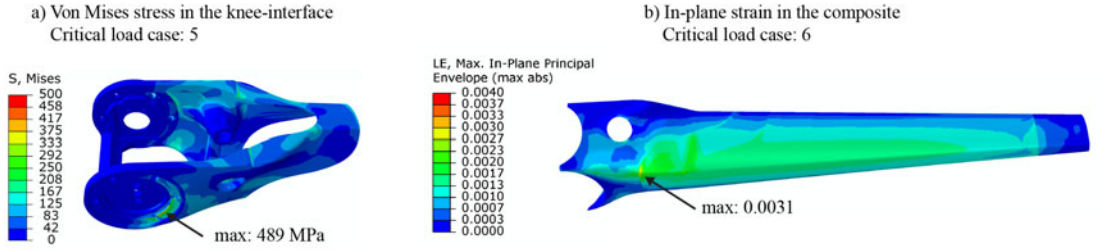

Figure 10. Simulation results for the critical load cases. Peak stresses are recorded for load case 5 in the bearing seats. Maximum in-plane laminate strain is found for load case 6 in the composite at the interface to the knee interface.

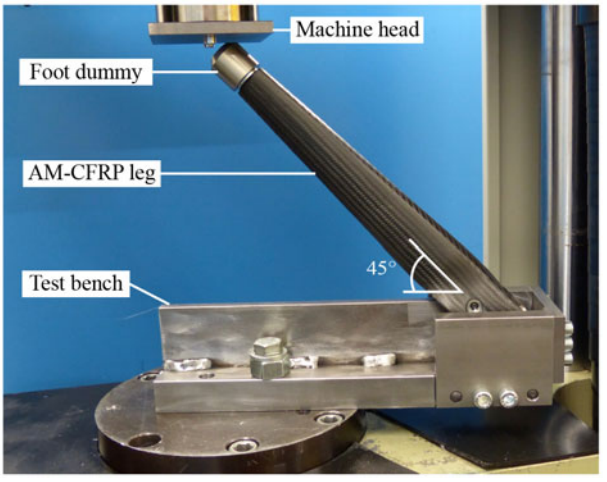

Figure 11. Ultimate strength test setup.

To determine the structurally critical location of the composite laminate, the maximum absolute value for the in-plane logarithmic strain (LE) was evaluated within each ply and calculated at the nodes of each element (Figure 10b). The maximum strain is observed for a combined tension and bending loading at 45° (load case 6) and amounts up to 0.31% in the transition of the composite to the knee interface. All values are below the allowables defined in Table 3 and therefore the design is acceptable.

4.2. Ultimate strength test result

A static test setup (Figure 11) replicating the compression–bending load case 3 (LC-3) was designed. LC-3 corresponds to a very common loading type during the operation of the robot which can easily be replicated using a tensile testing machine and a simple test setup. The purpose of the ultimate strength test is to identify the maximum loading capabilities of the structure and to verify the simulation model for operational load ranges. In this setup, the part is oriented at an angle of 45° to the horizontal. A static load was applied vertically into the foot dummy. The part was constrained at the bearing surfaces and at the shaft imitating

https://doi.org/10.1017/dsj.2019.16 Published online by Cambridge University Press

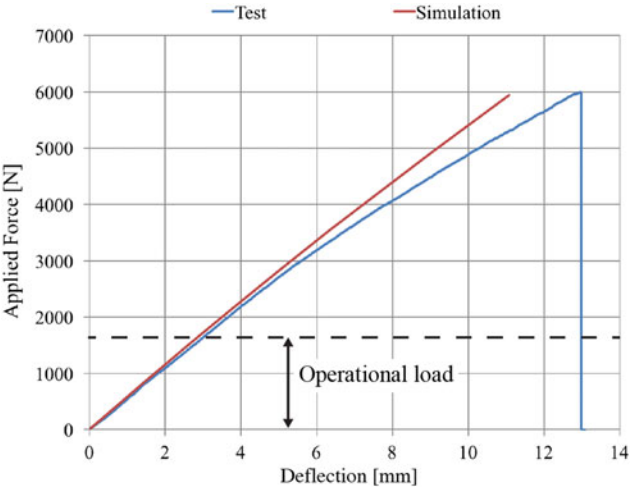

Figure 12. Comparison of experimental and simulation results for static loading.

the boundary conditions when mounted on the HyQ. The test load was applied using a Zwick Retroline DO131569 tensile testing machine with a displacement rate of 0.5 mm min^{-1} until failure occurred.

Figure 12 compares the test with simulation results. The force-displacement diagram shows a quasi-linear behavior until reaching a load of 2900 N where a loss in stiffness was observed. The structural integrity was maintained up to the ultimate load of 5994 N where abrupt failure occurred. The ultimate load significantly exceeded the operational load of 1600 N. In the simulation, the displacement of the load introduction point (foot interface) was taken as a reference. The simulation and the experiment are in good agreement for loads amounting to approximately 2900 N. In this area, the experimental stiffness of the structure amounts to 543 N mm^{-1} compared to 577 N mm^{-1} in the simulation, corresponding to a deviation of 6%. Non-linear effects may have occurred for loads above 2900 N which are not captured by the linear-elastic simulation. The steel shaft showed plastic deformation, which may have caused the discrepancy between the simulation and the experiment. Also, first failure in the CFRP may have occurred. However, both the simulation and the experiment highlight the structural integrity of the novel lower leg structure for loads within the operation envelope.

The failure locations depicted in Figure 13 show that the co-cured interface of the CFRP to the knee interface is critical. Mixed failure including laminate and adhesive failure is observed (a). We assume that the combined compression and bending loading induced shear and peel stresses which may have caused this type of failure. In addition, cracks in the laminate were observed next to the cutout of shaft (b). First, the co-cured area may have failed, leading to significant stress peaks and causing laminate fracture.

4.3. Weight

The final prototype weighs 298 g which corresponds to a reduction of 55% compared to 660 g of the reference design. The values are averaged over two

https://doi.org/10.1017/dsj.2019.16 Published online by Cambridge University Press

a) Mixed failure mode b) Laminate fracture

Figure 13. Laminate and mixed failure mode at the interface of the CFRP shell to the knee interface.

prototypes and rounded to the gram. One hundred and fifty-one grams are attributed to the knee interface, 24 g to the foot interface, 13 g to the shaft, 2 g to the sleeve, 104 g to the CFRP, and 4 g to the bolts and the washer. The weight savings arise from several factors. First, lightweight CFRP materials were used instead of aluminum. Second, the part count was significantly reduced through an integral design approach. The stopper and the bearing seats were integrated into the knee interface which allowed to eliminate joining elements. Moreover, one integral CFRP shell was employed compared to multiple machined elements requiring additional joints. Third, the freedom of design provided by the combination of AM with CFRP allowed to realize better load-oriented shapes which reduces the amount of un-utilized material.

5. Discussion

A manufacturing technique combining a 3D-printed shell with a granular structural support material for autoclave curing of CFRP was proposed and applied to a robotic structure. The main implications arise from separating shape, functionality, and structural curing support of the tooling. A major advantage of the proposed technique is the possibility for individualization and variety manufacturing of complex composite and hybrid structures without significantly increasing the manufacturing effort. The technique is design-driven and allows for rapid modifications and the realization of scalable product variants and families (Lei, Yao, Moon & Bi 2016). Design changes are mainly conducted in the digital environment and translated to digital production files for automated fabrication of shells and molds and near-net shape cutting of the reinforcements. Thus, the technique leverages the customization potential of 3D printing which is extended to composite manufacturing.

The technique is suitable for lot size one and small volume manufacturing of highly custom parts. However, scaling the technique to mid to high volumes is limited by the manual layup process, which is time-consuming for complex layups and geometries. While AM is automated and multiple layups can be cured in a single autoclave, the estimated time for performing the layup process typically scales proportionally with the production volume, and paralleling layup requires additional workforce.

In future, by leveraging a streamlined digital workflow for AM (Bonnard, Mognol & Hascoët 2010; Kim *et al.* 2015) in combination with a product and

https://doi.org/10.1017/dsj.2019.16 Published online by Cambridge University Press

manufacturing systems platform (Landahl *et al.* 2016), we expect to significantly improve design and manufacturing efficiency for complex variants. The proposed technique may be cost-competitive as the printing time is shorter and material consumption is lower compared to solid 3D-printed tooling. The separation of functions allows to process commercially available SLS materials in autoclave conditions instead of employing proprietary materials. Moreover, the technique allows to integrate accurate design features and thus to include additional functions into the shell considering only few manufacturing restrictions. By using SLS for the shell production, minimum wall thicknesses have to be considered for stable processing, but no support structures are required and the dimensional error is relatively small (Ibrahim *et al.* 2009; Salmi *et al.* 2013). Also, bigger shell structures may be possible by assembling separate shell segments.

The study revealed a few limitations. The tooling was tested in an autoclave curing cycle at 100 °C and a total of 3 bar pressure only. Many aerospace structures are cured at 180 °C and pressures ranging up to 10 bar. The limits of the processing window of the proposed technique are not yet known and the thermal behavior of the polymeric shell at extreme processing conditions was not investigated. The technique has worked well for the given geometry which was closed, elliptic, and approximately 30 cm in length. The filler material has well supported the shell during curing as no dents were observed. However, for a larger filling volume, the shell design may require modifications. The shell may be modeled as a plate with a distributed pressure loading. To avoid dents, the free length of the shell may have to be reduced for larger areas subjected to combined thermal and pressure loading. A simulation model for the prediction of the mechanical behavior of the shell and the filler subjected to thermo-mechanical loading is desired. The shell removal is critical to achieve a lightweight structure and requires part specific modifications. Studies on design guidelines for shell removal should be conducted by characterizing design parameters including the pre-determined breaking line geometry, breaking line length, and pitch, to name a few. The autoclave process was selected for curing, but the technique has the potential for extension to other composite manufacturing processes. 3D-printed shell elements filled with granular filler material may withstand high pressures and therefore have significant potential for applications in resin transfer molding and forming techniques, potentially allowing for a new scale of flexible high-volume manufacturing.

The simulation and the ultimate strength tests have shown that the co-cured interface of the CFRP to the titanium SLM part is critical to the load-bearing capability of the hybrid structure. Multi-material designs often exhibit stiffness discontinuities at interfaces which may yield stress peaks. Both AM and the prepreg technology offer potentials for the design of a bonding area with quasi-equal stiffness. The prepreg technology allows to tune the stiffness by varying materials, layup design, ply thickness, and orientation. The surface roughness of SLM may affect the bonding strength. Parameters influencing the surface roughness of SLM parts mainly include the building orientation and post-processing operations such as sand-blasting or roto-finishing. The process inherent (as-built) surface roughness could be beneficial to the bonding strength. Future joining concepts may use the peculiarities of AM or include novel 3D pin reinforcements that mechanically interlock with the reinforcements or resin modifications. These results also reveal potential for further weight savings in

https://doi.org/10.1017/dsj.2019.16 Published online by Cambridge University Press

the composite outside the interface. The application of fiber patches on a base laminate allows for optimization and tailoring of the structure and thus for improved utilization of the material. Optimal patch reinforcements may be found from numerical optimization (Kussmaul, Zogg & Ermanni 2018).

Weight savings of 55% were achieved compared to the reference structure. In addition, the mass moment of inertia could be reduced by roughly 70% as the center of gravity was moved close to the knee joint. Both characteristics should significantly impact the dynamic behavior of the actuation of the lower leg. Future studies should investigate how weight and mass moment of inertia reductions affect the robot's performance in terms of acceleration or power requirements.

6. Conclusions

A novel manufacturing technique for complex-shaped, hybrid composites was proposed. The key novelty is the removable tooling using a 3D-printed functional shell and a structural filler material for autoclave curing. The technique was applied to the lower leg structure of the HyQ robot: Carbon-fiber prepregs were co-cured to structural elements made by SLM, resulting in an intrinsic hybrid lightweight structure. The lower leg structure was tested in ultimate strength loading and successfully operated on the HyQ robot. Weight savings of 55% and significant lead time reduction indicate that the approach could be appropriate for complex-shaped, lightweight structures with potential for individualization.

Acknowledgments

We thank Dr. C. Semini and V. Barasuol of the Dynamic Legged Systems Lab of the Italian Institute of Technology for proposing the HyQ as a case study and for providing the experimental loads in Section 3.2. We thank Prof. P. Ermanni of ETH Zurich and Dr. M. Zogg of Inspire AG for providing access to the laboratory infrastructure. We also thank D. Fenner of ETH Zurich for his excellent craftsmanship on the milling machine. This research was supported by the Product Development Group Zurich, ETH Zurich.

References

3D Systems 2018 Duraform hst composite datasheet. https://www.3dsystems.com/materials/duraform-hst-composite/tech-specs.

Altropol 2018 Protosil rtv 245 silicone datasheet. http://www.altropol.de/wp-content/uploads/2016/11/E_RTV_245.pdf.

Ashby, M. & **Bréchet, Y.** 2003 Designing hybrid materials. *Acta Materialia* **51** (19), 5801–5821.

ASTM Std. F2792-12a 2012 'F2792-12a', *Standard Terminology for Additive Manufacturing Technologies ASTM International, West Conshohocken*.

Atzeni, E. & **Salmi, A.** 2012 Economics of additive manufacturing for end-usable metal parts. *The International Journal of Advanced Manufacturing Technology* **62** (9–12), 1147–1155.

Bernet, N., **Michaud, V.**, **Bourban, P.-E.** & **Månson, J.-A.** 2001 Commingled yarn composites for rapid processing of complex shapes. *Composites Part A: Applied Science and Manufacturing* **32** (11), 1613–1626.

https://doi.org/10.1017/dsj.2019.16 Published online by Cambridge University Press

Black, S. 2015 3d printing moves into tooling components. *CompositesWorld, Article Post June* **15**.

Bonnard, R., **Mognol, P.** & **Hascoët, J.-Y.** 2010 A new digital chain for additive manufacturing processes. *Virtual and Physical Prototyping* **5** (2), 75–88.

Campbell, F. C. 2003 *Manufacturing Processes for Advanced Composites*. Elsevier.

Concept Laser 2018 CL 41 TI ELI titanium alloy datasheet. https://www.concept-laser.de/fileadmin//user_upload/Datasheet_CL_41TI_ELI.pdf.

Dede, E. M., **Joshi, S. N.** & **Zhou, F.** 2015 Topology optimization, additive layer manufacturing, and experimental testing of an air-cooled heat sink. *Journal of Mechanical Design* **137** (11), 111403.

Duty, C. E., **Kunc, V.**, **Compton, B.**, **Post, B.**, **Erdman, D.**, **Smith, R.**, **Lind, R.**, **Lloyd, P.** & **Love, L.** 2017 Structure and mechanical behavior of big area additive manufacturing (BAAM) materials. *Rapid Prototyping Journal* **23** (1), 181–189.

Fernlund, G., **Rahman, N.**, **Courdji, R.**, **Bresslauer, M.**, **Poursartip, A.**, **Willden, K.** & **Nelson, K.** 2002 Experimental and numerical study of the effect of cure cycle, tool surface, geometry, and lay-up on the dimensional fidelity of autoclave-processed composite parts. *Composites Part A: Applied Science and Manufacturing* **33** (3), 341–351.

Fontana, F., **Marinelli, E.** & **Meboldt, M.** 2017 Selection of high-variety components for selective laser sintering: An industrial case study. In *International Conference on Additive Manufacturing in Products and Applications*, pp. 238–251. Springer.

Gibson, I., **Rosen, D. W.** & **Stucker, B.** 2010 Design for additive manufacturing. In *Additive Manufacturing Technologies*, pp. 299–332. Springer.

Gong, H., **Rafi, K.**, **Starr, T.** & **Stucker, B.** 2012 Effect of defects on fatigue tests of as-built ti-6al-4v parts fabricated by selective laser melting. In *Solid Freeform Fabrication Symposium*, pp. 499–506. University of Texas Austin.

Gutowski, T. G. P. 1997 *Advanced Composites Manufacturing*. John Wiley & Sons.

Hassen, A. A., **Lindahl, J.**, **Chen, X.**, **Post, B.**, **Love, L.** & **Kunc, V.** 2016 Additive manufacturing of composite tooling using high temperature thermoplastic materials. In *SAMPE Conference Proceedings, Long Beach, CA, May*, pp. 23–26.

Hosseini, S. 2012 Fatigue of ti-6al-4v. In *Biomedical Engineering-Technical Applications in Medicine*. InTech.

Ibrahim, D., **Broilo, T. L.**, **Heitz, C.**, **de Oliveira, M. G.**, **de Oliveira, H. W.**, **Nobre, S. M. W.**, **dos Santos Filho, J. H. G.** & **Silva, D. N.** 2009 Dimensional error of selective laser sintering, three-dimensional printing and polyjet models in the reproduction of mandibular anatomy. *Journal of Cranio-Maxillofacial Surgery* **37** (3), 167–173.

IIT 2018 Dynamic legged systems, istituto italiano di tecnologia. http://www.stratasys.com/solutions/additive-manufacturing/tooling/composite-tooling.

Kießling, R., **Ihlemann, J.**, **Riemer, M.**, **Drossel, W.-G.**, **Dittes, A.**, **Scharf, I.**, **Lampke, T.**, **Sharafiev, S.**, **Pouya, M.** & **Wagner, M.-X.** 2018 A process and load adjusted coating system for metallic inserts in hybrid composites. *Production Engineering* **12** (2), 249–257.

Kim, D. B., **Witherell, P.**, **Lipman, R.** & **Feng, S. C.** 2015 Streamlining the additive manufacturing digital spectrum: A systems approach. *Additive Manufacturing* **5**, 20–30.

Kirschman, C. & **Fadel, G. M.** 1998 Classifying functions for mechanical design. *Journal of Mechanical Design* **120** (3), 475–482.

Kussmaul, R., **Zogg, M.** & **Ermanni, P.** 2018 An optimality criteria-based algorithm for efficient design optimization of laminated composites using concurrent resizing and scaling. *Structural and Multidisciplinary Optimization* 1–16.

https://doi.org/10.1017/dsj.2019.16 Published online by Cambridge University Press

Landahl, J., **Levandowski, C.**, **Johannesson, H.**, **Söderberg, R.**, **Wärmefjord, K.**, **Carlson, J. S.**, **Kressin, J.**, **Isaksson, O.** & **Vallhagen, J.** 2016 Using product and manufacturing system platforms to generate producible product variants. *Procedia CIRP* **44**, 61–66.

Lei, N., **Yao, X.**, **Moon, S. K.** & **Bi, G.** 2016 An additive manufacturing process model for product family design. *Journal of Engineering Design* **27** (11), 751–767.

Li, H., **Taylor, G.**, **Bheemreddy, V.**, **Iyibilgin, O.**, **Leu, M.** & **Chandrashekhara, K.** 2015 Modeling and characterization of fused deposition modeling tooling for vacuum assisted resin transfer molding process. *Additive Manufacturing* **7**, 64–72.

Lossie, M. & **Van Brussel, H.** 1994 Design principles in filament winding. *Composites Manufacturing* **5** (1), 5–13.

Love, L. J., **Kunc, V.**, **Rios, O.**, **Duty, C. E.**, **Elliott, A. M.**, **Post, B. K.**, **Smith, R. J.** & **Blue, C. A.** 2014 The importance of carbon fiber to polymer additive manufacturing. *Journal of Materials Research* **29** (17), 1893–1898.

Lušić, M., **Schneider, K.** & **Hornfeck, R.** 2016 A case study on the capability of rapid tooling thermoplastic laminating moulds for manufacturing of cfrp components in autoclaves. *Procedia CIRP* **50**, 390–395.

Ma, S., **Gibson, I.**, **Balaji, G.** & **Hu, Q.** 2007 Development of epoxy matrix composites for rapid tooling applications. *Journal of Materials Processing Technology* **192**, 75–82.

Morena, J. J. 2011 Mold fabrications. In *Wiley Encyclopedia of Composites*, pp. 1–25. Wiley Online Library.

Nieschlag, J., **Ruhland, P.**, **Daubner, S.**, **Koch, S.-F.** & **Fleischer, J.** 2018 Finite element optimisation for rotational moulding with a core to manufacture intrinsic hybrid frp metal pipes. *Production Engineering* **12** (2), 1–9.

Orme, M. E., **Gschweitl, M.**, **Ferrari, M.**, **Madera, I.** & **Mouriaux, F.** 2017 Designing for additive manufacturing: Lightweighting through topology optimization enables lunar spacecraft. *Journal of Mechanical Design* **139** (10), 100905.

Ovtcharova, J., **Pahl, G.** & **Rix, J.** 1992 A proposal for feature classification in feature-based design. *Computers & Graphics* **16** (2), 187–195.

Paul, R., **Anand, S.** & **Gerner, F.** 2014 Effect of thermal deformation on part errors in metal powder based additive manufacturing processes. *Journal of Manufacturing Science and Engineering* **136** (3), 031009.

Salmi, M., **Paloheimo, K.-S.**, **Tuomi, J.**, **Wolff, J.** & **Mäkitie, A.** 2013 Accuracy of medical models made by additive manufacturing (rapid manufacturing). *Journal of Cranio-Maxillofacial Surgery* **41** (7), 603–609.

Schmelzle, J., **Kline, E. V.**, **Dickman, C. J.**, **Reutzel, E. W.**, **Jones, G.** & **Simpson, T. W.** 2015 (re) designing for part consolidation: understanding the challenges of metal additive manufacturing. *Journal of Mechanical Design* **137** (11), 111404.

Semini, C., **Tsagarakis, N. G.**, **Guglielmino, E.**, **Focchi, M.**, **Cannella, F.** & **Caldwell, D. G.** 2011 Design of hyq–a hydraulically and electrically actuated quadruped robot. *Proceedings of the Institution of Mechanical Engineers, Part I: Journal of Systems and Control Engineering* **225** (6), 831–849.

SGL Group 2018 Sigratex prepreg ce 1007-15-38 datasheet. http://www.carbon-vertrieb.com/shop/media/products/0447494001371540646.pdf.

Shin, K. C., **Lim, J. O.** & **Lee, J. J.** 2003 The manufacturing process of co-cured single and double lap joints and evaluation of the load-bearing capacities of co-cured joints. *Journal of Materials Processing Technology* **138** (1–3), 89–96.

Sriapai, T., **Walsri, C.** & **Fuenkajorn, K.** 2012 Effect of temperature on compressive and tensile strengths of salt. *ScienceAsia* **38** (2), 166–174.

https://doi.org/10.1017/dsj.2019.16 Published online by Cambridge University Press

Stratasys Ltd. 2017a Introduction to additive manufacturing for composites. http://www.stratasys.com/solutions/additive-manufacturing/tooling/composite-tooling.

Stratasys Ltd. 2017b Sacrificial tooling and mandrels composite part fabrication design guide. http://www.stratasys.com/solutions/additive-manufacturing/tooling/composite-tooling.

Tang, Y., **Hascoet, J.-Y.** & **Zhao, Y. F.** 2014 Integration of topological and functional optimization in design for additive manufacturing. In *ASME 2014 12th Biennial Conference on Engineering Systems Design and Analysis*, pp. V001T06A006–V001T06A006. American Society of Mechanical Engineers.

Türk, D.-A., **Brenni, F.**, **Zogg, M.** & **Meboldt, M.** 2017 Mechanical characterization of 3d printed polymers for fiber reinforced polymers processing. *Materials & Design* **118**, 256–265.

Türk, D.-A., **Einarsson, H.**, **Lecomte, C.** & **Meboldt, M.** 2018 Design and manufacturing of high-performance prostheses with additive manufacturing and fiber-reinforced polymers. *Production Engineering* **12** (2), 203–213.

Türk, D.-A., **Klahn, C.** & **Meboldt, M.** 2015 Combining additive manufacturing with cfrp composites: design potentials. In *Proceedings of the 20th International Conference on Engineering Design ICED*, pp. 27–31.

Türk, D.-A., **Kussmaul, R.**, **Zogg, M.**, **Klahn, C.**, **Leutenecker-Twelsiek, B.** & **Meboldt, M.** 2017 Composites part production with additive manufacturing technologies. *Procedia CIRP* **66**, 306–311.

Türk, D.-A., **Triebe, L.** & **Meboldt, M.** 2016 Combining additive manufacturing with advanced composites for highly integrated robotic structures. *Procedia CIRP* **50**, 402–407.

Upadhyay, M., **Sivarupan, T.** & **El Mansori, M.** 2017 3d printing for rapid sand casting a review. *Journal of Manufacturing Processes* **29**, 211–220.

Zhang, Y., **Pedersen, D. B.**, **Gøtje, A. S.**, **Mischkot, M.** & **Tosello, G.** 2017 A soft tooling process chain employing additive manufacturing for injection molding of a 3d component with micro pillars. *Journal of Manufacturing Processes* **27**, 138–144.

https://doi.org/10.1017/dsj.2019.16 Published online by Cambridge University Press